AGU PUBLICATIONS

Paleoceanography

RESEARCH ARTICLE
10.1002/2016PA003055

Key Points:
- Simulated surface temperatures show best fit to proxy-based temperature estimates in the midlatitudes
- In the high latitudes the data-model match can be improved by considering simulated summer rather than annual mean temperatures
- Gateway alterations improve the fit with the data only locally, at high altitudes in the North America

Correspondence to:
I. Niezgodzki,
ndniezgo@cyf-kr.edu.pl

Citation:
Niezgodzki, I., G. Knorr, G. Lohmann, J. Tyszka, and P. J. Markwick (2017), Late Cretaceous climate simulations with different CO_2 levels and subarctic gateway configurations: A model-data comparison, *Paleoceanography*, *32*, doi:10.1002/2016PA003055.

Received 17 NOV 2016
Accepted 21 AUG 2017
Accepted article online 28 AUG 2017

Late Cretaceous climate simulations with different CO_2 levels and subarctic gateway configurations: A model-data comparison

Igor Niezgodzki[1,2], Gregor Knorr[2,3], Gerrit Lohmann[2,4], Jarosław Tyszka[1], and Paul J. Markwick[5]

[1]ING PAN - Institute of Geological Sciences, Polish Academy of Sciences, Research Center in Kraków, Biogeosystem Modelling Laboratory, Kraków, Poland, [2]Alfred Wegener Institute, Helmholtz Centre for Polar and Marine Research, Bremerhaven, Germany, [3]School of Earth and Ocean Sciences, Cardiff University, Cardiff, UK, [4]MARUM-Center for Marine Environmental Sciences, University of Bremen, Bremen, Germany, [5]Getech, Leeds, UK

Abstract We investigate the impact of different CO_2 levels and different subarctic gateway configurations on the surface temperatures during the latest Cretaceous using the Earth System Model COSMOS. The simulated temperatures are compared with the surface temperature reconstructions based on a recent compilation of the latest Cretaceous proxies. In our numerical experiments, the CO_2 level ranges from 1 to 6 times the preindustrial (PI) CO_2 level of 280 ppm. On a global scale, the most reasonable match between modeling and proxy data is obtained for the experiments with 3 to 5 × PI CO_2 concentrations. However, the simulated low- (high-) latitude temperatures are too high (low) as compared to the proxy data. The moderate CO_2 levels scenarios might be more realistic, if we take into account proxy data and the dead zone effect criterion. Furthermore, we test if the model-data discrepancies can be caused by too simplistic proxy-data interpretations. This is distinctly seen at high latitudes, where most proxies are biased toward summer temperatures. Additional sensitivity experiments with different ocean gateway configurations and constant CO_2 level indicate only minor surface temperatures changes (<~1°C) on a global scale, with higher values (up to ~8°C) on a regional scale. These findings imply that modeled and reconstructed temperature gradients are to a large degree only qualitatively comparable, providing challenges for the interpretation of proxy data and/or model sensitivity. With respect to the latter, our results suggest that an assessment of greenhouse worlds is best constrained by temperatures in the midlatitudes.

1. Introduction

It has been recognized that the climate prevailing on Earth during the Cretaceous period was warmer than the present day [*Barron*, 1983; *Barron et al*., 1993; *DeConto et al*., 2000; *Frakes et al*., 2005]. The oceanic circulation was different than today [e.g., *Otto-Bliesner et al*., 2002; *Pucéat et al*., 2005] with deep-water formation sites located in the northwestern Pacific as suggested by Neodymium isotope data [*Hague et al*., 2012; *Moiroud et al*., 2013; *Donnadieu et al*., 2016]. Even though forcing boundary conditions (i.e., solar constant, aerosols, and SO_2), as well as continental configuration and vegetation were different than today, interest in understanding Cretaceous hot-house climates has increased as concerns grow that greenhouse conditions can return in a nondistant future due to rising CO_2 concentrations in the atmosphere [*Hay*, 2011].

Elevated CO_2 levels in the atmosphere have been considered as the main driver of the warm Cretaceous climate [e.g., *Hay and Floegel*, 2012]. Recent CO_2 level reconstructions based on different geobiological proxies (i.e., stomata, phytoplankton, liverworts, and nahcolite) suggest that CO_2 levels could be in the order of ~400 ppm and below ~800 ppm during the Cretaceous [*Royer et al*., 2012, Figure 1a]. However, a study of *Barclay and Wing* [2016] shows that estimating CO_2 level concentrations higher than 430 ppm from some biological proxies (stomatal index of fossil Ginkgo) should be used with caution. Earlier studies proposed CO_2 levels in the range of 560 ppm (2 × PI), to as high as 2800 ppm (10 × PI) [*Berner*, 1997] or even 4480 ppm (16 × PI) [*Monteiro et al*., 2012; *Poulsen and Zhou*, 2013]. However, the most typical range used recently in the climate simulations is 560–1680 ppm [e.g., *Otto-Bliesner et al*., 2002; *Donnadieu et al*., 2006; *Craggs et al*., 2012; *Hunter et al*., 2013]. Since considerable uncertainties exist for CO_2 levels reconstructions, it is natural to ask how modeled temperatures with different CO_2 scenarios compare to different proxy-based temperature reconstructions for the latest Cretaceous.

Furthermore, the equator-to-pole temperature gradient was reduced to ≤35°C [*Amiot et al*., 2004; *Hay*, 2008]. It is one of the greatest challenges related to the Late Cretaceous climate, to reasonably explain how this flat gradient could have been maintained. Different solutions were proposed to solve this intriguing problem. They include (but are not limited to) increased ocean heat transport [*Barron et al*., 1995], atmospheric latent heat transport [*Hay et al*., 1997], and different cloud properties than today [*Kump and Pollard*, 2008; *Upchurch et al*., 2015]. The focus in the proposed solutions to reconcile warm polar regions with moderate tropical temperatures under elevated CO_2 levels in the atmosphere was rather on different physical mechanisms of the climate system during a greenhouse world or model parameterization. Less focus was put on possible misinterpretations in proxy reconstructions.

However, especially in the northern polar region, proxy data provide diverging temperature estimates. The annual surface temperature reconstructions at the high latitudes in the database of *Upchurch et al*. [2015] differ by as much as ~14°C. Recent studies indicate that TEX_{86} data [*Jenkyns et al*., 2004] from the Arctic Ocean may not represent annual mean temperature but summer average temperature [*Davies et al*., 2009] or subsurface rather than surface [*Ho and Laepple*, 2016] conditions. Based on the integration of modeling results and proxy data from the Holocene, *Schneider et al*. [2010] and *Lohmann et al*. [2013] point out that the alkenone-based temperature reconstructions may register warm season temperature rather than annual mean in the high latitudes. Additionally, *Huber and Thomas* [2009] and *Lohmann et al*. [2013] suggest that the model-data mismatch can be caused by the different habitat depths of the marine organisms that record paleotemperatures.

In order to reconcile modeled high-latitude temperatures with the proxy-based temperature estimates, model studies applied elevated CO_2 concentrations in the atmosphere as a forcing boundary condition [*Bice et al*., 2006]. Then, the simulated temperatures in the tropics are relatively high and warmer than the proxy-based temperature reconstructions [*Shellito et al*., 2003]. The reason of this mismatch is unclear and different studies point to both uncertainties associated with the proxy records [*Pearson et al*., 2001; *Schouten et al*., 2003] as well as model uncertainties. The latter includes a selection of initial conditions (e.g., paleogeography), forcing boundary conditions (e.g., CO_2 concentrations in the atmosphere), and model parameterizations (such as cloud parameterization [*Upchurch et al*., 2015]).

The main goal of this study is to compare simulated surface temperatures with different CO_2 levels in the latest Cretaceous (~70 Ma) with recently published proxy-based temperature reconstructions during the corresponding time slice. We focus on the investigation of the shallow equator-to-pole temperature gradient in the Late Cretaceous that models cannot simulate except when cloud parameterization changes are applied [*Upchurch et al*., 2015]. Hence, we will test an alternative hypothesis whether part of a model-data mismatch in the high latitudes is created by the misinterpretations of the temperature proxies, in particular, their bias toward summer temperatures.

Furthermore, the simulation of warm continental interiors in the high latitudes has proven to be a challenge [*Craggs et al*., 2012]. *Donnadieu et al*. [2006] showed that paleogeography played an important role in the modulation of high-latitude climate during the Cretaceous. Therefore, another approach to reconcile the model-data discrepancies in the northern polar region was to simulate Late Cretaceous/Early Paleogene climate with different seaway configurations between the Arctic Ocean and North proto-Atlantic basin [*Roberts et al*., 2009; *Craggs et al*., 2012; *Hunter et al*., 2013]. However, there were discrepancies between these studies regarding the effect of the gateways on the Arctic Ocean climate. *Craggs et al*. [2012] and *Hunter et al*. [2013] found that the Arctic warmed when it became better connected with the global ocean, while *Roberts et al*. [2009] found a warming in the more isolated configuration. *Shellito et al*. [2009] simulated warming in the Arctic Ocean by ~4°C in the open configuration but during the Early Eocene. *Lunt et al*. [2016] attributed regional and global cooling to the closure of the Pacific-Arctic gateway.

Therefore, we will also investigate whether part of the discrepancies between modeled and reconstructed temperatures can be explained by uncertainties in the paleogeography that is used as a model boundary condition. We focus on the northern high latitudes to examine the influence of different seaway configurations in the Arctic Ocean region on the model-data mismatches. This area shows highly contradicting paleogeographic and paleobathymetric interpretations due to a scarcity of proxy data [*Cochran et al*., 2003; *Markwick and Valdes*, 2004; *Setoyama et al*., 2011a, 2011b, 2013; *Schröder-Adams*, 2014].

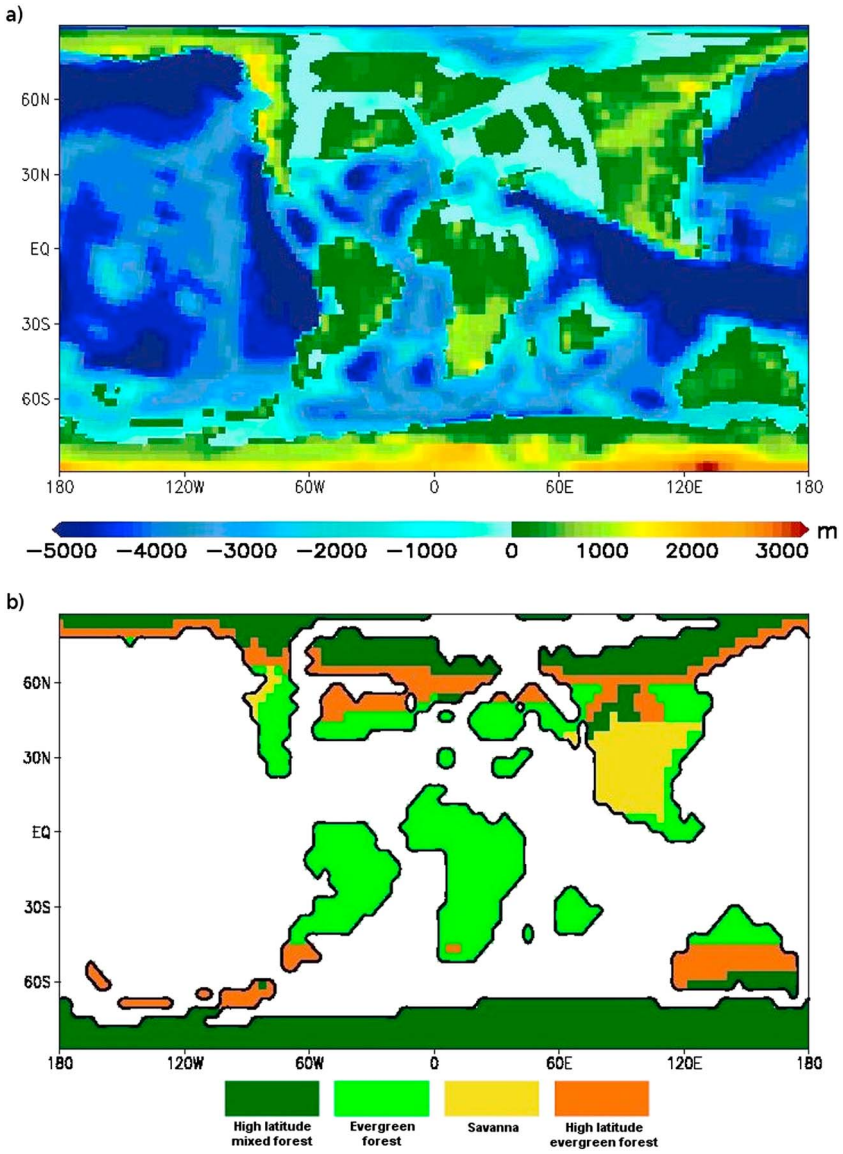

Figure 1. Model input boundary conditions as used in C-1120. (a) Bathymetry and orography in m and (b) plant functional types.

2. Methods

2.1. Experimental Design and Model Setup

We employ an atmosphere-ocean general circulation model (AOGCM) which was developed at the Max Planck Institute for Meteorology in Hamburg. The model has been successfully applied to test a variety of paleoclimate hypotheses, ranging from the late Paleocene/early Eocene and Oligocene climate [*Heinemann et al.*, 2009; *Walliser et al.*, 2016], the Miocene climate [*Knorr et al.*, 2011; *Knorr and Lohmann*, 2014; *Forrest et al.*, 2015; *Stein et al.*, 2016; *Huang et al.*, 2017; *Stärz et al.*, 2017], the Pliocene [*Stepanek and Lohmann*, 2012] as well as glacial [*Gong et al.*, 2013; *Zhang et al.*, 2013, 2014; *Köhler et al.*, 2014; *Abelmann et al.*, 2015] and interglacial climates [*Wei and Lohmann*, 2012; *Wei et al.*, 2012; *Lohmann et al.*, 2013; *Pfeiffer and Lohmann*, 2016]. In our Late Cretaceous simulations, we used the coupled ocean-atmosphere configuration with prescribed vegetation (described below).

The atmosphere component is the three-dimensional atmosphere general circulation model ECHAM5 [*Roeckner et al.*, 2003]. The model is run in T31/L19 resolution; i.e., the model contains 19 vertical layers and has a horizontal resolution of ~3.75°, which is equivalent to a resolution of ~400 km near the equator.

Table 1. Main Experimental Characteristics[a]

Experiment Acronym	CO_2 Level (ppm)	Global Mean Surface Temperature (°C)	Global RMSE (°C)	Low-Latitude RMSE (°C)	Midlatitude RMSE (°C)	High-Latitude RMSE (°C)
PI	280	14.66				
C-280	280	16.55	9.84	**3.70**	9.12	13.85
C-560	560	20.96	7.25	4.50	6.33	10.32
C-840	840	24.41	5.70	7.26	4.25	7.20
C-1120	1120	26.03	**5.54**	8.83	**3.89**	5.68
C-1400	1400	27.36	5.90	10.03	4.24	**5.06**
C-1680	1680	30.21	7.67	12.45	6.48	5.14
WIS-0	1120	27.00	6.22	9.65	4.86	**5.45**
HUD-0	1120	25.90	5.74	8.75	4.19	6.06
NS-47	1120	25.97	**5.52**	**8.74**	**3.84**	5.77

[a]RMSE (columns 4–7) calculated between the reconstructed and modeled temperatures for each experiment globally and with the divisions for low, middle, and high latitudes. For comparison, a global mean surface temperature of PI experiment is presented. The best fit is shown in bold.

The hydrological discharge submodel is included within the atmosphere component [*Hagemann and Dümenil*, 1998a, 1998b; *Hagemann and Gates*, 2003]. The model simulates lateral freshwater fluxes over the land surface, which is separated into an overland flow, baseflow, and riverflow. Furthermore, in our Late Cretaceous setup glaciers are absent.

The Max Planck Institute Ocean Model (MPI-OM) is the ocean component of the AOGCM [*Marsland et al*., 2003]. MPI-OM is a primitive equation and free surface ocean model with hydrostatic and Boussinesq assumptions. The model includes a dynamic-thermodynamic sea ice submodel [*Hibler*, 1979]. The MPI-OM runs in a GR30/L40 configuration. This represents 40 vertical layers and a formal horizontal resolution of 3.0° × 1.8°. The thickness of the vertical layers changes with depth. Eight layers are within the first 90 m depth and 20 layers are in the first 600 m. MPI-OM is integrated on an orthogonal curvilinear grid with two poles, which are located over land. The Ocean-Atmosphere-Sea Ice-Soil (OASIS) coupler is responsible for coupling between the atmosphere and the ocean components [*Valcke*, 2013].

We use the paleogeography of *Markwick and Valdes* [2004] for the geographic boundary condition (Figure 1a). This Late Cretaceous paleogeography is only one of the series of paleogeographies compiled by *Markwick* [2007] representing periods of the Earth history with different paleoshorelines. For consistency in all our studies, we use paleogeographies from the same source as an input boundary conditions in all of our simulations.

In order to set up a global vegetation distribution for the Late Cretaceous, we utilize a plant functional type (PFT) reconstruction prepared by *Sewall et al*. [2007]. The map contains eight plant functional types and land ice. We reduce the number of PFTs in our Cretaceous setup from eight to four (Figure 1b). We specify the following land surface conditions in the parameter values for each PFT: surface albedo, surface roughness length, field capacity of soil, forest ratio, leaf area index, fractional vegetation cover, soil wetness, and soil data flags (Food and Agriculture Organization soil map) [cf. *Hagemann et al*., 1999]. The first six parameter values for many different PFTs are described in *Hagemann* [2002]. Parameters of Food and Agriculture Organization data flags follow *Stärz et al*. [2016]. Soil wetness, which is simulated by AOGCM is initialized with values adopted from *Stärz et al*. [2016].

The exact values of orbital parameters for the pre-Cenozoic times are unknown, due to chaotic behavior of the solar system [*Laskar et al*., 2004]. For our experiments, we fixed the orbital parameters to the values from the year 800 A.D. They represent the values from the beginning of the millennial run (externally forced simulation of the world from 800 to 1800 A.D.). The solar constant is set to the present day value (1367 W/m^2) for first 1770 years for the model spin-up. Subsequently, it is reduced by 1% to a value of 1353.33 W/m^2 [*Gough*, 1981], in line with other modeling studies [*Poulsen et al*., 2003; *Sellwood and Valdes*, 2006; *Donnadieu et al*., 2006; *Poulsen and Zhou*, 2013].

We set up six experiments which differ only in the atmospheric CO_2 concentration (Table 1) and an additional three experiments with different gateway configurations between the Arctic Ocean and North proto-Atlantic basin (Table 2, Figures 5a, 5c, and 5e). The atmospheric concentration of CH_4 and N_2O are set at the PI level in

Table 2. Changes in the Paleogeography of Three Experiments With Respect To *Markwick and Valdes* [2004] Paleogeography

Experiment Acronym	CO_2 Level (ppm)	Changes With Respect To *Markwick and Valdes* [2004] Paleogeography
C-1120	1120	*Markwick and Valdes* [2004]
WIS-0	1120	Western Interior and Hudson Seaways closed
HUD-0	1120	Hudson Seaway closed
NS-47	1120	Nares Strait open (47 m deep)

each experiment (650 ppb and 270 ppb, respectively). Experiment NS-47 reflects possible gateway configuration during the Late Cretaceous [*Schröder-Adams*, 2014]. Experiments WIS-0 and HUD-0 represent paleogeographies which likely evolved from the Maastrichtian (~70 Ma) paleogeography toward the Cr-Pg boundary [*Cochran et al*., 2003; *Schröder-Adams*, 2014]. We choose them for comparison with the data, because most of the available proxies come from a region around these gateways. Therefore, we can simultaneously investigate the effect of the gateways on the local temperature changes and also in comparison with data. Additionally, we compare some of our results with the preindustrial control experiment. The setup of this experiment is identical as used earlier by *Knorr et al*. [2011]. We have integrated the experiment in total for ~8300 years and take the last 100 years for the analyses.

The simulation C-1120 is initialized with horizontally uniform ocean temperature (of 1°C) and salinity (of 34.8 psu) profiles and subsequently is run for 4800 model years. The experiments C-280 and C-560 were restarted (with a simultaneous abrupt CO_2 level change) from C-1120 after ~1770 years, C-840 after ~3800 years, and C-1400 and C-1680 after ~4300 years. The experiment WIS-0 was restarted from C-1120 after ~3000 years, NS-47 after ~4000 years, while HUD-0 was restarted from WIS-0 after ~4000 years. Each experiment was further modeled to the year 4800. The analysis is based on the climatology calculated from the last 100 years of the simulations.

The evolution of the sea surface temperature is shown in Figure 2 since the model year 1770 (for simulations C-280, C-560, and C-1120). We can observe that at the surface the temperatures are in quasi-equilibrium for all simulations apart from the experiment C-1680, where the temperature is still increasing. However, this experiment is already much too warm (see section 4 and Table 1) and further integration would simply amplify the mismatch. Furthermore, the deep ocean is not in full equilibrium in any of the experiments, which might produce differences in fully equilibrated simulations. However, we show that the averaged temperature in the upper 1.5 km water column of the spin-up experiment C-1120 (C-1120_deep on Figure 2) is in equilibrium. The model years ~3030–3400 in C-1120 have not been stored and hence they are not shown in the figure. Given the time evolution of the parameter, this does not limit our results and conclusions.

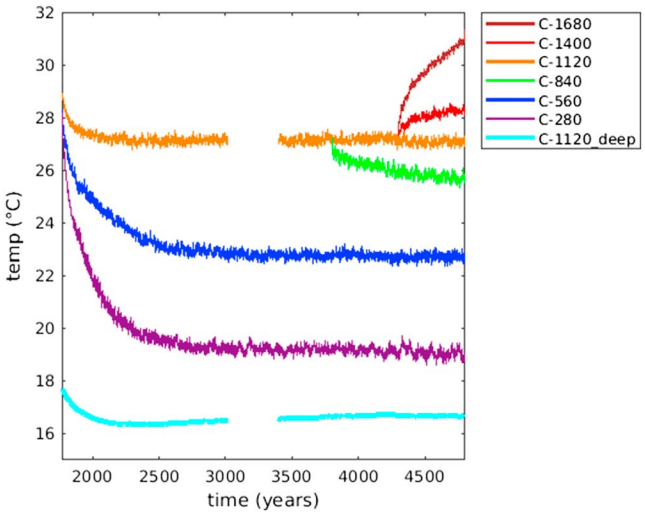

Figure 2. The evolution of sea surface temperature for six experiments. Additionally, the evolution of the temperature in the upper 1.5 km water column (marked as C-1120_deep) in the spin-up experiment C-1120 is shown.

2.2. Model—Data Comparison Methodology

We compare our results with different proxy data-based temperature reconstructions compiled by *Upchurch et al*. [2015]. They project the locations of the proxy data (Part 1 in the Data Repository and Figure 1 in their study) on the modified paleogeography used in *Upchurch et al*. [1999]. This Maastrichtian paleogeography differs from the *Markwick and Valdes* [2004] paleogeography used in our simulations. In consequence, some terrestrial proxy data from *Upchurch et al*. [2015] are located over the ocean (and vice versa) on paleogeography of *Markwick and Valdes* [2004]. In order to provide a consistent model-data comparison, we move the location

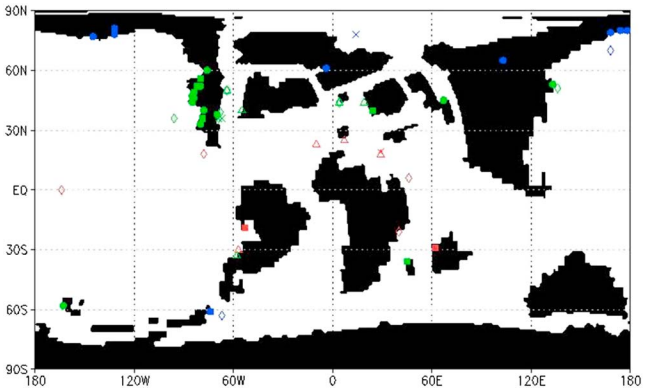

Figure 3. Locations of data points [*Upchurch et al.*, 2015] on the land-sea mask as provided by *Markwick and Valdes* [2004]. Red color indicates low, green middle, and blue high latitudes. Filled squares indicate terrestrial $\delta^{18}O$, filled circles paleobotanical, open triangles fish enamels $\delta^{18}O$, open diamonds marine $\delta^{18}O$, and crosses TEX_{86} proxies.

of such data points from the ocean (land) to the nearest land (ocean) point. The final locations of the data points (which are taken to the model-data comparison) on *Markwick and Valdes* [2004] land-ocean configuration, as used in our study, are shown in Figure 3. Furthermore, the database of *Upchurch et al.* [2015] contains locations, where different temperature reconstruction methods or calibration techniques are used for the same proxy. If different calibrations are applied for a reconstruction method, an average for the specific proxy and method is calculated based on the individual calibrations. This value is averaged with all available temperature reconstructions from other methods at a particular location.

For comparison with the proxy data from the Arctic Ocean (14°E, 78°N), in C-280 and C-560 we take the sea surface temperatures (SST) instead of surface temperatures because the formation of sea ice in that region has an important effect on surface temperature. The same holds for the marine data located between Antarctica and South America (67°W, 27°S) but only in C-280. Furthermore, for comparison with WIS-0, we remove all marine data points, where the gateway closure introduces the new land points.

3. Results

In the following subsections, we compare our results (Figures 4 and 5) with the proxy data and with other modeling studies. We make this comparison both globally as well as in the low, middle, and high latitudes separately.

3.1. Global Scale

The calculated annual global mean surface temperature for the different simulations is shown in Table 1 (col. 3). The surface temperature in all Late Cretaceous simulations exceeds the surface temperature of the PI simulation. The global mean surface temperature in C-1120 is ~11.3°C higher than that in the PI control experiment. These results fit to the upper surface temperature range proposed by *DeConto* [1996] and *Barron et al.* [1995], who suggested that Late Cretaceous temperatures were warmer than today by about 7–14°C and 6–12°C, respectively. *Donnadieu et al.* [2006] simulated mean surface temperature during the Maastrichtian with the 1120 ppm level of ~8°C higher than the present day. This is less than the difference in global mean surface temperature simulated in our C-840 experiment, which is ~9.7°C higher than that in PI. Furthermore, our simulated global mean surface temperature in C-560 is ~4.4°C higher than that in C-280. *Hunter et al.* [2008] simulate a warming of ~2.3°C for a CO_2 rise in the atmosphere from 280 ppm to 560 ppm in their Maastrichtian experiments.

In order to compare the modeling results with the proxy data, we plot scatter diagrams of modeled surface temperatures against the corresponding proxy-based temperature reconstructions (Figure 6). Furthermore, we calculate a root-mean-square error (RMSE) for each CO_2 level (Table 1, col. 4). Globally the best match with the proxy data is obtained in the simulation C-1120. However, the simulated surface temperatures in C-840 and C-1400 show only a marginally less favorable match with the reconstructed temperatures compared to C-1120. The CO_2 level of 840 ppm as used in C-840 is in reasonable agreement with the CO_2 concentration as estimated from the geological data [*Royer et al.*, 2012]. The CO_2 level of 1120 ppm as used in C-1120 is close to the CO_2 reconstruction, while 1400 ppm as used in C-1400 probably represents a relatively high value [*Breecker et al.*, 2010; *Franks et al.*, 2014].

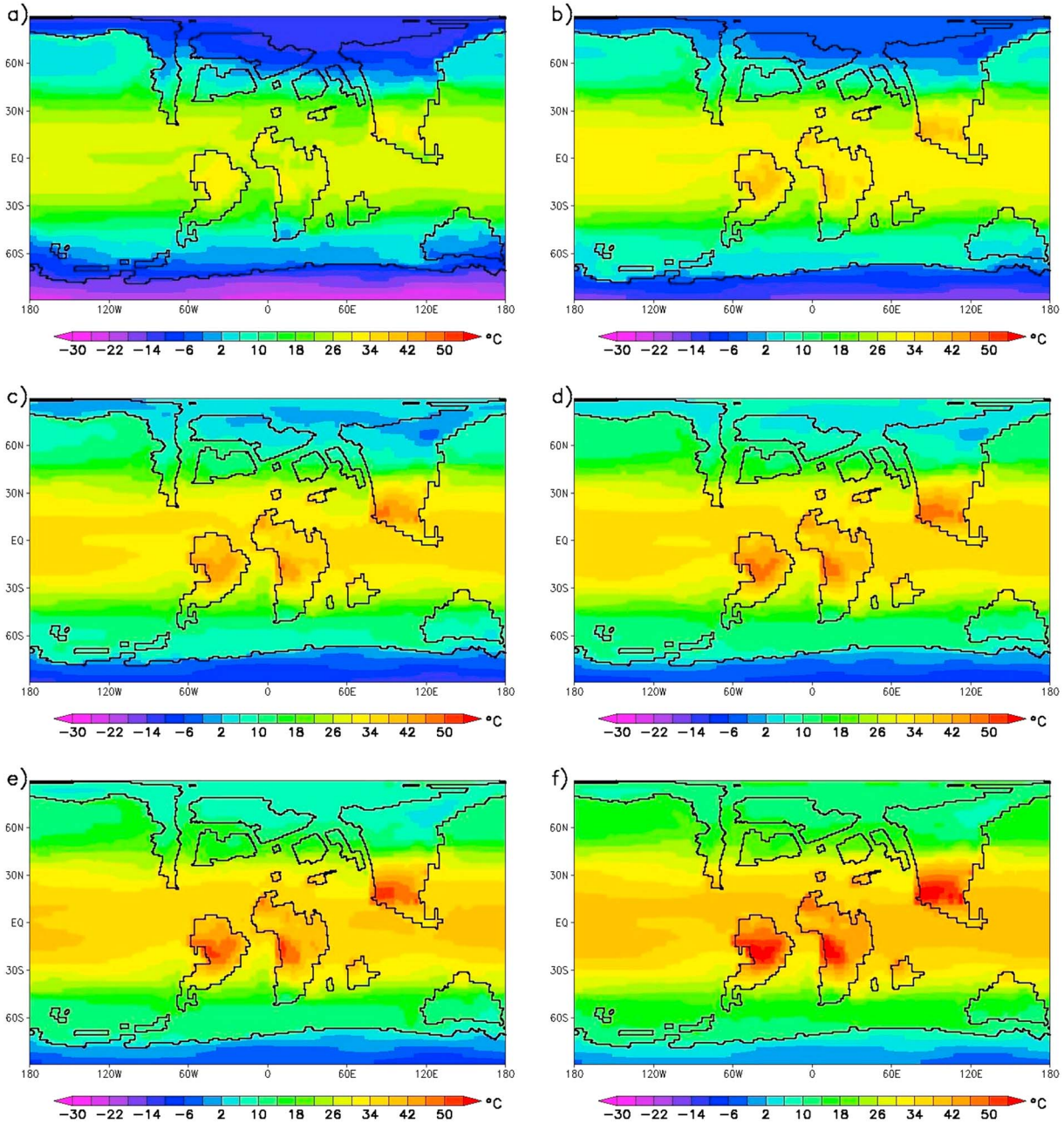

Figure 4. Maastrichtian surface temperatures in °C depicted for experiments (a) C-280, (b) C-560, (c) C-840, (d) C-1120, (e) C-1400, and (f) C-1680.

3.2. Low Latitudes

The comparison of model-data temperatures via the scatter diagrams (Figure 6) shows that in the low latitudes (latitude belt 30°S to 30°N) the closest match with the data is obtained in the simulations with low CO_2 levels. Calculated RMSE confirm (Table 1, col. 5) that in the tropics the temperatures in C-280 are the closest to those reconstructed from the proxy data.

The annual mean surface temperatures in local areas in South America, Africa, and Asia in C-280 are up to ~33–35°C. However, with the higher CO_2 levels, the surface temperatures in the same regions are above 45°C in C-840, ~50°C in C-1120 and C-1400, and they can reach maximum values of ~55–56°C in C-1680 (Figure 4). *Winguth et al*. [2010] simulate SATs of ~50°C in the subtropical Africa and South America for the

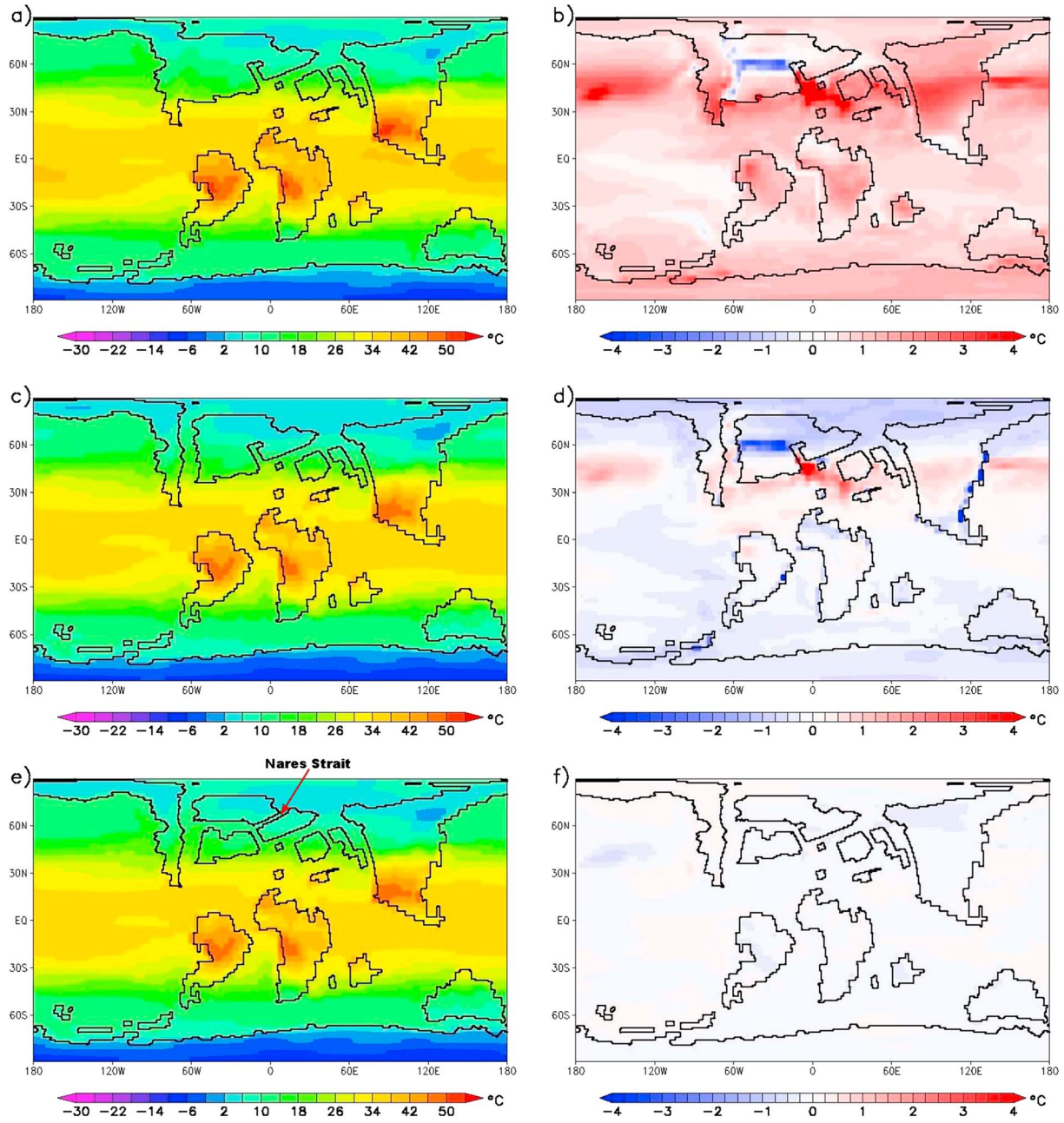

Figure 5. Maastrichtian surface temperatures in °C depicted for (a) WIS-0, anomaly (b) WIS-0 experiment minus C-1120 experiment, (c) HUD-0 anomaly (d) HUD-0 experiment minus C-1120 experiment, (e) NS-47, anomaly (f) NS-47 experiment minus C-1120 experiment.

Paleocene-Eocene Thermal Maximum and in the simulation with 2240 ppm CO_2 level. Furthermore, the surface temperatures over the tropical western Pacific Ocean are mostly >35°C in C-840, C-1120, and C-1400 and >39°C in C-1680. It is warmer than in the simulations of *Otto-Bliesner et al.* [2002] with CO_2 level of 1680 ppm and *Hunter et al.* [2008] with 1120 ppm. Proxy-based temperature reconstructions indicate lower SSTs in the tropical oceans. *Pearson et al.* [2001] estimate SSTs of ~28–32°C based on foraminifera shells. *Schouten et al.* [2003] reconstruct SSTs of ~32–36°C during early Late Cretaceous by applying the TEX_{86} method to crenarchaeotal membrane lipids. Using the same method *Dumitrescu et al.* [2006] reconstructed SSTs of ~33–36°C during early Aptian, while *Forster et al.* [2007] SSTs of ~35–36°C during Turonian.

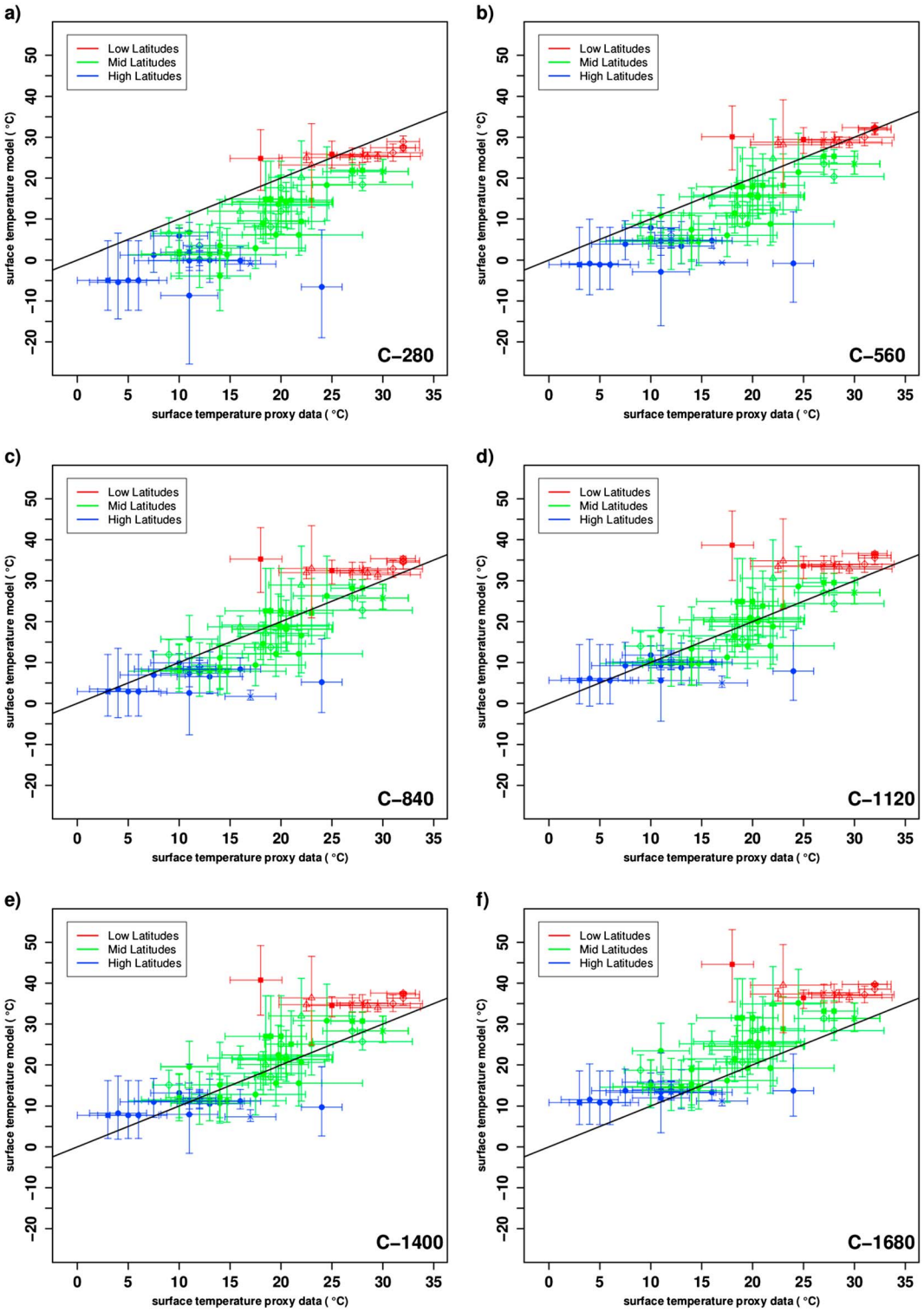

Figure 6. Proxy-based temperature reconstructions in °C plotted against modeled surface temperatures in (a) C-280, (b) C-560, (c) C-840, (d) C-1120, (e) C-1400, and (f) C-1680. Vertical error bars represent seasonal range (summer and winter temperatures), while horizontal uncertainty range in the data reconstructions. The straight black line represents 1:1 line match. The meaning of symbols as in Figure 3.

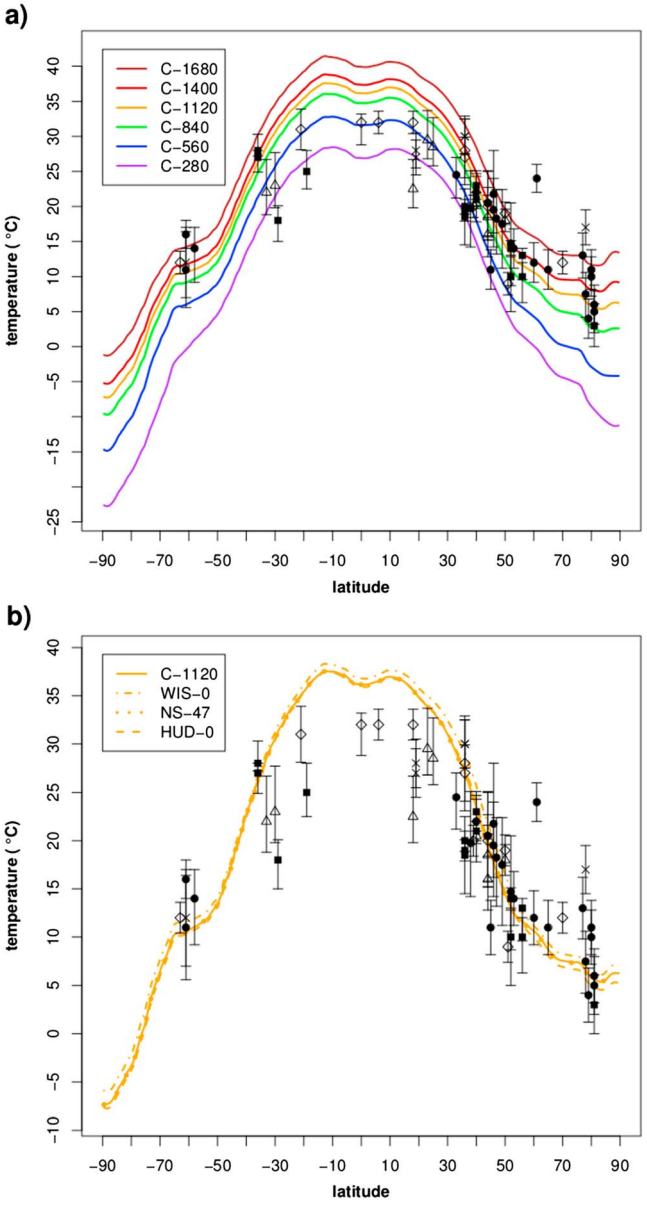

Figure 7. Modeled zonal mean temperatures with (a) different CO_2 levels and (b) different gateway configurations in °C versus proxy data with the error bars. The meaning of symbols as in Figure 3.

In Figure 7a we can observe that in the low latitudes all proxy-based temperature reconstructions are below the zonal annual mean surface temperatures (ZMT) in C-840, as well as in all other experiments with higher CO_2 levels. In C-1120 the simulated ZMT is outside the upper range of uncertainties of proxy data from the low latitudes.

3.3. Midlatitudes

In the midlatitudes (latitude belt between 30° and 60° in each hemisphere) the most reasonable match with the reconstructions is achieved within the 840–1400 ppm CO_2 range (Figure 6 and Table 1). The best match is obtained in C-1120 as revealed by calculation of RMSE (Table 1, col. 6).

Over the midlatitude ocean surface temperatures in both hemispheres in C-1120 show a similar pattern and values to simulated temperatures by *Otto-Bliesner et al.* [2002] and *Hunter et al.* [2008]. Additionally, these temperatures are in agreement with the temperature estimates obtained by *Linnert et al.* [2014] using TEX_{86} analysis as a paleothermometer. In C-1120 the temperatures of 21°C (the minimum temperature which allows for a formation and development of coral reefs) are found in the latitude belt of ~40–45° on both hemispheres, in agreement with modeled temperatures by *Otto-Bliesner et al.* [2002].

The temperatures over the southwestern part of North America (the region where the bulk of the proxy data comes from) are ~5–10°C in C-280. Over the same region in C-560 surface temperatures are ~2–4°C higher than that in C-280, ~6–9°C higher in C-840, ~8–11°C higher in C-1120, ~9–12°C higher in C-1400, and ~13–17°C higher in C-1680. Furthermore, the temperatures in WIS-0 over this region are ~1–3°C higher than in C-1120 (Figure 5b). In NS-47 the temperatures are almost identical to C-1120 (Figure 5f). In HUD-0 differences in temperature are $<$1°C in the magnitude compared to C-1120 (Figure 5d). Additionally, in WIS-0 we detect a warming of ~2.5–4°C compared to C-1120 over the midlatitude Pacific Ocean and Asia. This warming can be as high as ~8°C to the south of Greenland in WIS-0 and ~6°C in HUD-0.

In Figure 7a we can observe that most of the temperature reconstructions at the midlatitudes locations fit between the ZMTs of C-560 and C-1680. Furthermore, all ZMTs are within the range of uncertainties of the proxy data. However, it should be emphasized that only the CO_2 level of 560 ppm and 840 ppm (C-560 and C-840) are in the range of reconstructed CO_2 concentrations [*Royer et al.*, 2012; *Franks et al.*, 2014].

3.4. High Latitudes

In the high latitudes (latitude belt between 60° and 90° in each hemisphere) a reasonable match with the data is obtained in the experiments with the higher CO_2 levels. The best match is obtained in the simulation C-1400 (Table 1, col. 7). However, other experiments with high CO_2 levels, i.e., C-1120 and C-1680 also show a reasonable match with the temperature reconstructions.

Our simulated surface temperatures in C-1120 in the Arctic Ocean (~5–7°C) are similar to the SSTs simulated by *Otto-Bliesner et al*. [2002]. *Hunter et al*. [2008] simulate SSTs of ~2°C. However, both *Otto-Bliesner et al*. [2002] and *Hunter et al*. [2008] employ 1680 ppm CO_2 level in their simulations rather than a 1120 ppm as used in C-1120. *Roberts et al*. [2009] simulate an Early Paleogene Arctic Ocean SST average of ~0.7°C and ~1.5°C in their experiments with open and closed gateways, using a CO_2 level of ~1200 ppm (~4.3 × PI). Proxy-based temperature estimates for the Arctic Ocean range from annual SSTs of ~15°C [*Tarduno et al*., 1998; *Jenkyns et al*., 2004] to temperatures (< 0°C around the coast of Arctic Ocean) which allow for a formation of intermittent sea ice in the ocean [*Amiot et al*., 2004; *Davies et al*., 2009].

A comparison among modeled surface temperatures with different CO_2 concentrations (Figure 4) shows that the CO_2 level has an important effect on the magnitude of the surface temperature in the high latitudes. In C-280 and C-560 surface temperatures <0° (apart from the entire Arctic Ocean) are found over the whole of Antarctica, as well as the northern parts of Asia and North America. Furthermore, in C-280 we detect surface temperatures <0°C over the southern part of Australia and along the coast of Antarctica (between the eastern coast of Australia and west of Africa). In C-840 and C-1120 annual mean surface temperatures <0°C are detected only over Antarctica and in the small region in the Northeast Asia. In C-1400 and C-1680 temperatures below freezing are found only in the southern part of Antarctica.

Gateways alterations have relatively minor effect on the surface temperatures in the Arctic Ocean. In WIS-0 we detect warming in the Arctic Ocean of ~0.5–1°C compared to C-1120 (Figure 5b), in the HUD-0 cooling of ~0.5–1°C (Figure 5d), while in NS-47 minor changes are observed compared to C-1120 (Figure 5f).

4. Discussion

Below we discuss potential reasons for differences between the modeled and reconstructed temperature estimates.

4.1. Global Scale: Shortage of Global Solutions

Our simulated temperature increase for a CO_2 level doubling, from 280 ppm to 560 ppm, is within the upper range of climate sensitivity proposed by *Solomon et al*. [2007]. Based on a combination of constraints from observations and model simulations, they estimate a warming of ~2–4.5°C for a CO_2 increase from 280 ppm to 560 ppm for modern conditions. However, we must point out that a comparison to our results is not straightforward due to different input boundary conditions, like continental configuration and ice sheets. Nevertheless, our model seems to be relatively sensitive to CO_2 changes compared to other climate models. This has also been detected in Model Intercomparison Projects for Eocene [*Lunt et al*., 2012] and Pliocene timeslices [*Haywood et al*., 2013] where the model applied in our study is one of the most sensitive models to CO_2 changes.

Furthermore, for the temperature reconstructions based on oxygen isotopes from fish tooth enamels [*Pucéat et al*., 2007; *Ounis et al*., 2008], the recalibration techniques of *Pucéat et al*. [2010] and *Lécuyer et al*. [2013] are provided in the database of *Upchurch et al*. [2015]. *Pucéat et al*. [2010] recalibrations are based on a larger number of specimens; therefore, they might be more correct (G. R. Upchurch, personal communication, 2016). Moreover, the terrestrial oxygen-based temperature reconstructions are usually colder than other temperature estimates from the same region [*Upchurch et al*., 2015]. This suggests that they may show a bias toward cold month mean temperatures, due to different sources of water for the crocodiles, as well as limitations in the understanding of the fractionation process of precipitation in the greenhouse world (references cited in *Upchurch et al*. [2015, Supplementary Information]).

We are able to reduce the RMSE globally, in the simulations with CO_2 level ≥ 560 ppm, by removing all terrestrial isotope-based temperature estimates and *Lécuyer et al*. [2013] recalibrations (Table 3, col. 2). The best match is then obtained in C-1120 and C-1400. The CO_2 level of 1400 ppm, as set in C-1400 cannot be

Table 3. RMSE Calculated Between the Modeled Surface Temperatures and the Proxy-Based Temperature Estimates Without Oxygen Terrestrial Isotope Reconstructions and *Lécuyer et al*. [2013] Recalibrations (White Background)[a]

Experiment Acronym	Global RMSE (°C)	Low-Latitude RMSE (°C)	Midlatitude RMSE (°C)	High-Latitude RMSE (°C)	High-Latitude RMSE (°C)	High-Latitude RMSE (°C)
C-280	10.55	3.76	9.92	14.15	10.12	8.35
C-560	7.69	**2.21**	7.07	10.61	7.66	6.59
C-840	5.56	4.54	4.64	7.43	5.79	6.14
C-1120	**4.88**	5.85	3.83	5.83	5.41	6.77
C-1400	**4.88**	6.97	**3.74**	5.08	5.81	7.59
C-1680	6.22	9.35	5.4	**4.91**	7.08	9.26

[a]High-latitude RMSE calculated between the reconstructed and modeled warm months (boreal AMJJAS) surface temperatures (green background) and summer (JJA) surface temperatures (yellow background). The best fit is shown in bold.

reconciled with proxy-based CO_2 reconstructions, but a 1120 ppm CO_2 level as used in C-1120 and 840 ppm CO_2 level as used in C-840 are close to the estimates from the data [see *Breecker et al*., 2010].

It seems that comparison of the model-proxy results gives just a rough estimate of realistic CO_2 scenarios that are applicable on the global scale. Main reasons for the lack of simple and global solutions among limitations are a scattered and incomplete proxy record; time averaging of proxies that represent longer time intervals; limited long-distance proxy correlations (especially between marine and terrestrial facies); complex preservation bias; diagenesis [see, e.g., *Kowalewski*, 1996*; Retallack*, 1998*; Behrensmeyer et al*., 2000].

4.2. Low Latitudes: Implications of Dead Zone

The best match with the data in the low latitudes is obtained for the simulation (C-280) where a CO_2 level is lower than the recent estimates for the Late Cretaceous based on a compilation of different geological data [*Breecker et al*., 2010]. However, atmospheric CO_2 level reconstructions based on stomatal proxies indicate that CO_2 level could be close to preindustrial at the end of Cretaceous [*Royer et al*., 2012, Figure 1a]. Furthermore, *Lefebvre et al*. [2013] suggest that the location of North Africa and northern South America in the tropics around the Cr-Pg boundary should have supported increased weathering, thus promoting a low background CO_2 level in the atmosphere. However, we must stress that experiment C-280 does not provide a reasonable match with the proxy data in the middle and high latitudes (Table 1); therefore, this low CO_2 concentration should be used with caution.

Our simulated regional surface temperature is well above 42°C in the high CO_2 levels scenarios. This is too high to sustain any form of plant life [*Hay and Floegel*, 2012] and is not supported by geological data [*Amiot et al*., 2004]. We, therefore, take into account the Dead Zone Effect that is a regional life-limiting mechanism, including extreme temperatures that inhibit most life forms [*Hay and Floegel*, 2012]. Heat stress in the tropics strongly limits photosynthesis that slowdowns between 35°C and 42°C. Daytime temperatures above 42°C are critical for plant life survival [*Hay and Floegel*, 2012]. Such temperatures could have sustained plan and animal life in the tropics. *Chumakov et al*. [1995] predict that in the Maastrichtian the tropical South America and South-East Asia were inhabited by dinosaurs. It would be unlikely for them to thrive at the temperatures that are simulated in our experiments with high CO_2 levels. Thus, we assume that the lower to moderate CO_2 levels are more realistic than the high CO_2 concentrations with respect to the specific dead zone criterion.

If we consider higher CO_2 concentrations, the warm bias in the tropical regions suggests that some physical processes might be missing in the climate models. Another possibility is that the mismatch between model-data temperature estimates might be biased by an incorrect proxy data interpretation. A removal of all *Lécuyer et al*. [2013] recalibrations and terrestrial isotope proxies from the database reduces the RMSE in low latitudes to the value as low as 2.21°C and 4.54°C in C-560 and C-840, respectively. These CO_2 levels are within the range of predicted CO_2 concentration for the Late Cretaceous [*Breecker et al*., 2010]. Furthermore, in C-1120 the RMSE is reduced from 8.38°C to 5.85°C. This indicates that the model-data mismatch in the low latitudes can be partly explained by uncertainties in terrestrial isotope-based

temperature reconstructions. Therefore, these proxy-based temperature reconstructions should be used with caution in the tropics.

Our additional gateways configuration changes between the Arctic Ocean and North proto-Atlantic basin have only minor influences on temperatures in the tropics and thus cannot explain the model-data bias. Furthermore, Figure 7b also shows that the ZMTs in the tropics are relatively insensitive to the northern high-latitude seaway alterations and local changes even amplify the model-data mismatch as in WIS-0 over South America.

4.3. Midlatitudes: Actualistic Conditions

The midlatitudes in the Northern Hemisphere present the best proxy record due to their better accessibility and dense sampling [see *Upchurch et al*., 2015]. Furthermore, the temperate paleoclimates did not experience extreme conditions that might be expected in low and high latitudes. Such actualistic conditions enable application of proxies calibrated to recent conditions. This is therefore not surprising that midlatitudinal reconstructions are more reliable and show most reasonable match between the model results and the proxy data (Tables 1 and 3 and Figures 6 and 7).

In the midlatitudes, most of the proxy-based temperatures are derived from the paleobotanical, terrestrial oxygen isotope and fish tooth enamel data [*Upchurch et al*., 2015]. The paleobotanical methods are mostly Climate Leaf Analysis Multivariate Program (CLAMP) and Leaf Margin Analysis (LMA). CLAMP and terrestrial oxygen isotope proxies usually give colder results than other reconstructions. This suggests that they may be cold biased or represent minimum temperatures (G. R. Upchurch, personal communication, 2016). However, most of our modeled terrestrial temperatures in C-1120 from the western part of North America (the region where the vast majority of the proxy data from the Northern Hemisphere midlatitudes are located) are in close agreement (or are even in the lower range of sampling error) with the lower temperature reconstructions. This reasonable match with colder temperature estimates might partly result from the elevation in that region as set in our model configuration (as high as ~1750 m), which represents the early formation of the Rocky Mountains. However, the timing of the formation and uplift of the mountains is still debated [*Dettman and Lohmann*, 2000]. If the suggested elevation of ~2.5–3 km [*Dettman and Lohmann*, 2000] at the end of Cretaceous is true, then the colder proxy-based temperature reconstructions from western North America (as simulated in C-1120) may be more correct due to the lapse rate effect. Likewise, the other way round, if we assume that the warmer temperature reconstructions (based on more reliable LMA method) were correct, then these elevations might be too high. However, *Markwick* [2007] points out that the cold bias in simulated temperatures at high altitudes might result from a coarse elevational resolution in climate models.

The gateway configuration changes also not fully resolve the mismatches between the model and data (Figure 7b). The temperatures in the WIS and western North America as modeled in HUD-0 and NS-47 are almost identical to C-1120 (Figures 5d and 5f). In WIS-0 we simulate warmer temperatures (Figure 5b) compared to C-1120. This helps to improve the agreement between the model and data for most of the proxies located at higher altitudes. However, for the majority of the proxies at lower elevations, the mismatch is greater in WIS-0 than in C-1120 because simulated temperatures (which were already too high in C-1120) are even higher in this experiment. Furthermore, a lack of data in the regions where the temperature differences are large (midlatitude Asia and the Pacific Ocean) in WIS-0 compared to C-1120 makes it difficult to verify the gateways effect in these regions.

4.4. High Latitudes: Nonactualistic Perspective

A notorious problem in climate models is the simulation of temperatures in the high latitudes [*Craggs et al*., 2012; *Poulsen and Zhou*, 2013; *Upchurch et al*., 2015] that are inconsistent (too cold) with reconstructions [*Brady et al*., 1998]. As a result, relatively high CO_2 levels are often used to reconcile the modeled and reconstructed temperatures in the high latitudes, but simultaneously in the tropics too warm temperatures are simulated compared to reconstructions. *Huber and Caballero* [2011] point out (based on the Eocene model-data comparison) that this approach can be justified and the mismatches in the tropics can result from the uncertainties in temperature reconstructions in the low latitudes. In our simulations, we seem to face the same challenge, as the best match between model and the data in the high latitudes is achieved for C-1400. However, the CO_2 concentration as used in this simulation is not supported by the geological data for the

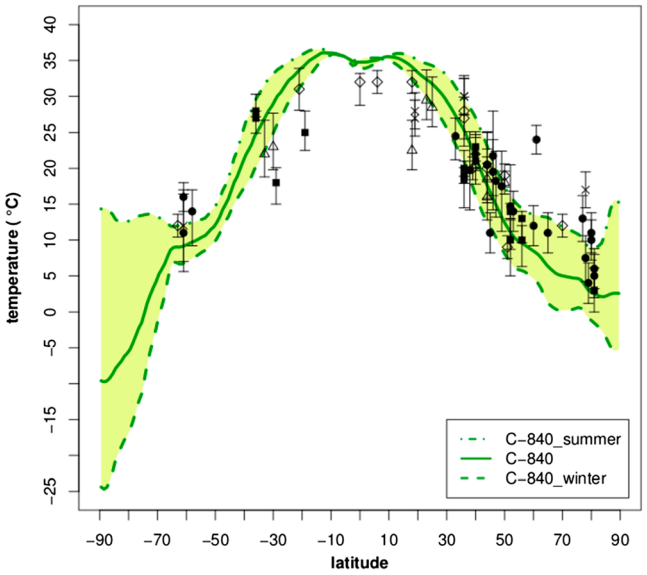

Figure 8. Modeled zonal mean annual, local summer, and local winter temperatures for C-840 in °C versus proxy data with the error bars. The meaning of symbols as in Figure 3.

Late Cretaceous. In contrast to the low latitudes (where our model clearly simulates too high temperatures for CO_2 levels ≥ ~840 ppm), in the Arctic Ocean region, the mismatch between the proxies and modeling results can be partly reconciled by uncertainties in proxy data interpretation. On the other hand, uncertainties of the cloud properties during greenhouse world and problems with the cloud parameterization in the models can lead to the underestimated warming caused by a radiative forcing effect of polar clouds [*Kump and Pollard*, 2008; *Huber and Thomas*, 2009; *Kiehl and Shields*, 2013; *Upchurch et al*., 2015].

In the database, only one single proxy exists from the Arctic Ocean [*Jenkyns et al*., 2004]. The temperature reconstruction of that proxy is ~10°C higher than our modeled temperature in C-1400. However, the TEX_{86} temperature reconstruction method has been recognized as maximum temperatures rather than annual mean [*Davies et al*., 2009]. *Spicer and Herman* [2010] also dispute the estimation of *Jenkyns et al*. [2004], and they propose a temperature of ~14.5°C (based on the CLAMP method) as a warm month mean temperature for the Arctic Ocean coastal region at 82°N during the Maastrichtian. A recent study of *Ho and Laepple* [2016] indicates an error in the calibration of the TEX_{86}-based temperature reconstructions as they are calibrated to the surface ocean, even though they likely formed in subsurface conditions. As a consequence, TEX_{86} temperature reconstructions should be used with caution [*Ingalls*, 2016]. *Ho and Laepple* [2016] suggest that the absolute value of TEX_{86}-derived temperatures should be approximately halved and that they actually represent subsurface temperatures. This would decrease the value of the only proxy from the Arctic Ocean in *Upchurch et al*. [2015] from 17°C to ~8.5°C, which is close to simulated subsurface (~200 m depth) temperatures in C-1400.

Furthermore, proxy-based temperature reconstructions in the high latitudes provide a very wide range of temperatures (Figure 7) (see *Upchurch et al*. [2015] for details). All of these reconstructions are warmer than the temperatures simulated in C-840, and most of them lie within the range of temperatures as simulated by C-1120 and C-1680. On the Northern Hemisphere in the high latitudes, most of the reconstructions come from paleobotanical data (CLAMP and LMA). Some of these data are highly reliable; nevertheless, *Greenwood* [1991] points out that terrestrial vascular plant proxies are usually biased toward humid sites, such as swamps, river deposits, and flood deposits that might mask the original average temperature records. This so-called "the freshwater-margin effect" [*Peppe et al*., 2011] may affect paleotemperature reconstructions. According to *Skelton* [2003], the leaf diversity in the Campanian and Maastrichtian near-polar environments was so low that paleobotanical proxies are unreliable. *Herman et al*. [2016] also point out too low plant diversity to allow the use of leaf morphology to estimate climate parameters in the early Maastrichtian of the Northern Alaska.

Recent studies [*Schneider et al*., 2010; *Lohmann et al*., 2013] point out that in the high latitudes some marine temperature reconstructions (i.e., alkenone-based) are biased toward warm seasons. *Davies et al*. [2009] suggest that the *Jenkyns et al*. [2004] TEX_{86} temperature reconstruction can rather represent summer temperature, not an annual mean. Furthermore, during long polar days in the Cretaceous plants had optimal growing conditions with permanent sunlight access and mild summer temperatures from 10°C to 20°C (Figure 8) [e.g., *Spicer and Herman*, 2010]. Such conditions favored and selected vascular plants that colonized completely nonactualistic niche that is missing in icehouse conditions. Furthermore, there is an evolutionary

aspect of paleobotanical data interpretations. *Little et al*. [2010] state that paleobotanical proxies indicate an overall limited ability to reconstruct climate precisely due to its nonrandom phylogenetic signal. Although we know that in the Late Cretaceous early angiosperm plants colonized the higher latitudes, being well adapted to such warm conditions [e.g., *De Boer et al*., 2012], nevertheless, their temperature estimates cannot be approximated based on recent analogs. It means that the Cretaceous plants were on another, a much earlier evolutionary track that may be difficult to interpret based on actualistic calibrations. Therefore, we suspect that calibration of paleobotanical proxies in such conditions is a great challenge. This is very likely that their recorded temperatures might be strongly biased toward warmer values.

Therefore, we have compared our simulated local warm months (AMJJAS, from April to September; Table 3, col. 7) and summer temperatures (JJA; Table 3, col. 9 and Figure 8) with temperature reconstructions in the high latitudes. Overall, we obtain a worse match for the high CO_2 scenarios, while for the experiments with the low CO_2 levels we reduce RMSE.

Another approach is to modify model formulations/parameterizations for warmer climate states. *Kump and Pollard* [2008] assumed that the concentration of cloud condensation nuclei in the atmosphere during the preindustrial world was lower. This could increase the droplet radii of the liquid clouds and also increase the precipitation efficiency of these clouds. In their simulation with 1120 ppm CO_2 level and changed cloud parameterization *Kump and Pollard* [2008] successfully simulated warming in the high latitudes during the Cretaceous compared to the simulation with a standard cloud parameterization. The same approach was used by *Kiehl and Shields* [2013] to simulate an Eocene climate in agreement with data. *Upchurch et al*. [2015] modified properties of clouds and obtained in the Cretaceous the best match with the data in the simulations with the CO_2 level of 560 ppm. Applying these cloud parameterization changes together with simultaneous consideration in the high latitudes of modeled summer temperatures rather than annual mean might further improve the match between the reconstructed and simulated temperatures in the high latitudes. However, this is beyond the scope of the present paper.

The removal of terrestrial oxygen-based reconstruction has relatively minor effect on RMSE in the high latitudes (Table 3 col. 5). However, additional removal of an outlier located in southern Greenland (record #11 in the database of *Upchurch et al*. [2015]) reduces the RMSE to a value as low as 4.22°C, 3.62°C, and 4.28°C in C-1120, C-1400, and C-1680, respectively. This suggests that this reconstruction might be treated with caution in the model-data comparison. *Wolfe and Upchurch* [1987] argue that this high temperature could result from a strong western boundary current in the region where this proxy was located. Furthermore, *Otto-Bliesner and Upchurch* [1997] and *Upchurch et al*. [1999] indicate that high-latitude forest contributed to polar warmth during Late Cretaceous. *Hunter et al*. [2013] point out that, in particular, in the high latitudes vegetation cover can result in a regional warming by up to ~10°C. This might suggest that different, local vegetation cover existed in the region where this outlier is located. Another possibility is that this site was located slightly more to the south of Greenland and this surface temperature reconstruction is representative for periods when Hudson Seaway was closed, as, e.g., in WIS-0 and HUD-0. In these simulations, we observe a warming just to the southern tip of Greenland, which is up to ~8°C warmer than in C-1120 (Figures 5b and 5d).

Gateways changes cannot explain the mismatches between the model and the data in the high latitudes. We can observe only small surface temperature changes compared to C-1120 (Figure 7b). Comparison of surface temperature anomalies (Figures 5b, 5d, and 5f) shows that the changes caused by the gateways configuration alterations in the Arctic Ocean are $<$ ~1°C in magnitude. This shows that seaway configuration changes can only provide a local improvement between the model and the data-based temperature.

To summarize, the proxy data-model mismatch can be caused by both, uncertainties in the proxy data interpretation, e.g., seasonality, recording depth, different methods of proxy calibrations, recording system, time-averaging, correlation problems, as well as deficiencies of the model, e.g., coarse resolution, unresolved costal dynamics, cloud parameterization, and warming effect of polar clouds in the high latitudes (see *Huber and Thomas* [2009] for overview). More proxy data are needed from the sparsely explored regions such as open oceans (i.e., the Pacific Ocean), high latitudes (i.e., Antarctica and Arctic Ocean) and continental regions in the Southern Hemisphere (i.e., Australia, South America, and Africa). In order to improve model-data comparison and reduce uncertainties in the proxy data interpretations, a natural next step would be to simulate the global $\delta^{18}O$ isotopic distribution, using, e.g., a fully coupled Earth system model, that is complemented by a stable water isotope model [e.g., *Werner et al*., 2011].

5. Conclusions

We simulate the latest Cretaceous climate with six different CO_2 levels (280–1680 ppm) and conduct three additional sensitivity tests with different gateway configurations between a North proto-Atlantic basin and Arctic Ocean. Globally the best match with the proxy data is obtained for the simulation with a CO_2 level of 1120 ppm. A comparable match is also achieved in the simulation with a 840 ppm that is within the range of CO_2 reconstructions for the latest Cretaceous.

Similar to previous modeling studies we are unable to reconcile low-CO_2 scenarios with moderate temperatures in the tropics and relatively warm polar regions. However, our analyses show that

1. The best fit between the modeled and reconstructed temperatures is at midlatitudes as revealed by separation of the global data-model mismatch into low-, middle-, and high-latitude components;
2. At high latitudes and for the low-CO_2 scenarios the match between the reconstructed and modeled temperatures can be improved by considering simulated local summer temperatures rather than annual mean temperatures;
3. Changes in ocean gateways at middle and high latitudes improve the model-data match only locally/regionally, and the improvement on larger global scales is limited.

These findings imply that modeled and reconstructed temperature gradients are to a large degree only qualitatively comparable, providing a challenge for the interpretation of proxy data in terms of the recording season or even recording depth (see a discussion for the Holocene [*Lohmann et al*., 2013]). Finally, our results imply that an assessment of the greenhouse world temperature with elevated CO_2 concentrations (the global climate sensitivity to atmospheric CO_2 perturbations) might be best constrained by temperature changes in the midlatitudes. This suggestion is further motivated by the best proxy representation in the midlatitudes due to high sampling density and best calibration based on actualistic environments. This is in contrast to low and high latitudes, which in the greenhouse world experience more extreme and nonactualistic conditions.

Acknowledgments
We thank three anonymous reviewers and C. Shellito for the invaluable suggestions and constructive comments. We gratefully acknowledge the help of Garland R. Upchurch who has provided us valuable additional information and explanations about proxy data interpretations and related with them uncertainties. We would like to thank Stefan Hagemann for the preparation of the adjustments of the HD model for our Cretaceous setup. We are grateful to the AWI Computing Center for providing the supercomputing resources for carrying out the simulations. Igor Niezgodzki's research is funded from the resources of the National Science Center in Poland based on the decision DEC-2012/07/N/ST10/03419, the DAAD (57130104 in 2015/16) and ATLAB Project (EU FP7 REGPOT, 285989). Funding for Gerrit Lohmann and Gregor Knorr was provided by Helmholtz Society (PACES program Topic 3 WP2) and for Jarosław Tyszka by ING PAN (PALEOECOLOGY internal project). We thank all researchers who provided the proxy data. All data used are listed in the references. Modeling data are available at 'https://doi.pangaea.de/10.1594/PANGAEA.879763'.

References

Abelmann, A., et al. (2015), The seasonal sea-ice zone in the glacial Southern Ocean as a carbon sink, *Nat. Commun.*, *6*, 8136, doi:10.1038/ncomms9136.

Amiot, R., C. Lécuyer, E. Buffetaut, F. Fluteau, S. Legendre, and F. Martineau (2004), Latitudinal temperature gradient during the Cretaceous Upper Campanian–Middle Maastrichtian: $\delta^{18}O$ record of continental vertebrates, *Earth Planet. Sci. Lett.*, *226*(1–2), 255–272, doi:10.1016/j.epsl.2004.07.015.

Barclay, R. S., and S. L. Wing (2016), Improving the ginkgo CO_2 barometer: Implications for the early Cenozoic atmosphere, *Earth Planet. Sci. Lett.*, *439*, 158–171, doi:10.1016/j.epsl.2016.01.012.

Barron, E. J. (1983), A warm, equable Cretaceous: The nature of the problem, *Earth Sci. Rev.*, *19*(4), 305–338, doi:10.1016/0012-8252(83)90001-6.

Barron, E. J., P. J. Fawcett, D. Pollard, S. Thompson, A. Berger, and P. Valdes (1993), Model simulations of Cretaceous climates: The role of geography and carbon dioxide [and discussion], *Philos. Trans. R. Soc. London, Ser. B*, *341*(1297), 307–316, doi:10.1098/rstb.1993.0116.

Barron, E. J., P. J. Fawcett, W. H. Peterson, D. Pollard, and S. L. Thompson (1995), A "simulation" of mid-cretaceous climate, *Paleoceanography*, *10*(5), 953–962, doi:10.1029/95PA01624.

Behrensmeyer, A. K., S. M. Kidwell, and R. A. Gastaldo (2000), Taphonomy and paleobiology, *Paleobiology*, *26*(sp4), 103–147, doi:10.1666/0094-8373(2000)26[103:TAP]2.0.CO;2.

Berner, R. A. (1997), The rise of plants and their effect on weathering and atmospheric CO_2, *Science*, *276*(5312), 544–546, doi:10.1126/science.276.5312.544.

Bice, K. L., D. Birgel, P. A. Meyers, K. A. Dahl, K. U. Hinrichs, and R. D. Norris (2006), A multiple proxy and model study of Cretaceous upper ocean temperatures and atmospheric CO_2 concentrations, *Paleoceanography*, *21*, PA2002, doi:10.1029/2005PA001203.

Brady, E. C., R. M. DeConto, and S. L. Thompson (1998), Deep water formation and poleward ocean heat transport in the warm climate extreme of the Cretaceous (80 Ma), *Geophys. Res. Lett.*, *25*(22), 4205–4208, doi:10.1029/1998GL900072.

Breecker, D. O., Z. D. Sharp, and L. D. McFadden (2010), Atmospheric CO_2 concentrations during ancient greenhouse climates were similar to those predicted for A.D. 2100, *Proc. Natl. Acad. Sci.*, *107*(2), 576–580, doi:10.1073/pnas.0902323106.

Chumakov, N. M., M. A. Zharkov, A. B. Herman, M. P. Doludenko, N. N. Kalandadze, E. L. Lebedev, A. G. Ponomarenko, and A. S. Rautian (1995), Climatic belts of the mid Cretaceous time, *Stratigr. Geol. Correl.*, *3*(3), 241–260.

Cochran, J. K., N. H. Landman, K. K. Turekian, A. Michard, and D. P. Schrag (2003), Paleoceanography of the Late Cretaceous (Maastrichtian) Western Interior Seaway of North America: Evidence from Sr and O isotopes, *Palaeogeogr. Palaeoclimatol. Palaeoecol.*, *191*(1), 45–64, doi:10.1016/S0031-0182(02)00642-9.

Craggs, H. J., P. J. Valdes, and M. Widdowson (2012), Climate model predictions for the latest Cretaceous: An evaluation using climatically sensitive sediments as proxy indicators, *Palaeogeogr. Palaeoclimatol. Palaeoecol.*, *315–316*, 12–23, doi:10.1016/j.palaeo.2011.11.004.

Davies, A., A. E. S. Kemp, and J. Pike (2009), Late Cretaceous seasonal ocean variability from the Arctic, *Nature*, *460*(7252), 254–258, doi:10.1038/nature08141.

De Boer, H. J., M. B. Eppinga, M. J. Wassen, and S. C. Dekker (2012), A critical transition in leaf evolution facilitated the Cretaceous angiosperm revolution, *Nat. Commun.*, *3*, 1221, doi:10.1038/ncomms2217.

DeConto, R. M. (1996), Late Cretaceous climate, vegetation and ocean interactions: An earth system approach to modeling an extreme climate, PhD thesis, Univ. of Colorado, Boulder.
DeConto, R. M., E. C. Brady, J. Bergengren, and W. W. Hay (2000), Late Cretaceous climate, vegetation, and ocean interactions, in *Warm Climates in Earth History*, pp. 275–297, Cambridge Univ. Press, Cambridge, U. K.
Dettman, D. L., and K. C. Lohmann (2000), Oxygen isotope evidence for high-altitude snow in the Laramide Rocky Mountains of North America during the Late Cretaceous and Paleogene, *Geology*, *28*(3), 243–246, doi:10.1130/0091-7613(2000)28<243:OIEFHS>2.0.CO;2.
Donnadieu, Y., R. Pierrehumbert, R. Jacob, and F. Fluteau (2006), Modelling the primary control of paleogeography on Cretaceous climate, *Earth Planet. Sci. Lett.*, *248*(1–2), 426–437, doi:10.1016/j.epsl.2006.06.007.
Donnadieu, Y., E. Pucéat, M. Moiroud, F. Guillocheau, and J. F. Deconinck (2016), A better-ventilated ocean triggered by Late Cretaceous changes in continental configuration, *Nat. Commun.*, *7*, 10316, doi:10.1038/ncomms10316.
Dumitrescu, M., S. C. Brassell, S. Schouten, E. C. Hopmans, and J. S. S. Damsté (2006), Instability in tropical Pacific sea-surface temperatures during the early Aptian, *Geology*, *34*(10), 833–836, doi:10.1130/G22882.1.
Frakes, L. A., J. E. Francis, and J. I. Syktus (2005), *Climate Modes of the Phanerozoic*, Cambridge Univ. Press, Cambridge, U. K.
Franks, P. J., D. L. Royer, D. J. Beerling, P. K. Van de Water, D. J. Cantrill, M. M. Barbour, and J. A. Berry (2014), New constraints on atmospheric CO_2 concentration for the Phanerozoic, *Geophys. Res. Lett.*, *41*, 4685–4694, doi:10.1002/2014GL060457.
Forrest, M., J. T. Eronen, T. Utescher, G. Knorr, C. Stepanek, G. Lohmann, and T. Hickler (2015), Climate-vegetation modelling and fossil plant data suggest low atmospheric CO_2 in the late Miocene, *Clim. Past*, *11*, 1701–1732, doi:10.5194/cp-11-1701-2015.
Forster, A., S. Schouten, M. Baas, and J. S. S. Damsté (2007), Mid-Cretaceous (Albian–Santonian) sea surface temperature record of the tropical Atlantic Ocean, *Geology*, *35*(10), 919–922, doi:10.1130/G23874A.1.
Gong, X., G. Knorr, G. Lohmann, and X. Zhang (2013), Dependence of abrupt Atlantic meridional ocean circulation changes on climate background states, *Geophys. Res. Lett.*, *40*, 3698–3704, doi:10.1002/grl.50701.
Gough, D. O. (1981), *Solar Interior Structure and Luminosity Variations, in Physics of Solar Variations*, pp. 21–34, Springer, Dordrecht, Netherlands.
Greenwood, D. R. (1991), The taphonomy of plant macrofossils, in *The Processes of Fossilization*, pp. 141–169, Columbia Univ. Press, New York.
Hagemann, S. (2002), An improved land surface parameter dataset for global and regional climate models, *Report 336*, Max-Planck-Institut für Meteorologie, Hamburg.
Hagemann, S., and L. Dümenil (1998a), A parametrization of the lateral waterflow for the global scale, *Clim. Dyn.*, *14*(1), 17–31, doi:10.1007/s003820050205.
Hagemann, S., and L. Dümenil (1998b), Documentation for the hydrological discharge model, *DKRZ Technical Report No. 17*, Deutsches Klimarechenzentrum, Hamburg.
Hagemann, S., and L. D. Gates (2003), Improving a subgrid runoff parameterization scheme for climate models by the use of high resolution data derived from satellite observations, *Clim. Dyn.*, *21*(3–4), 349–359, doi:10.1007/s00382-003-0349-x.
Hagemann, S., M. Botzet, L. Dumenil, and B. Machenhauer (1999), Derivation of global GCM boundary conditions from 1 km land use satellite data, *Report 289*, Max-Planck-Institut für Meteorologie, Hamburg.
Hague, A. M., D. J. Thomas, M. Huber, R. Korty, S. C. Woodard, and L. B. Jones (2012), Convection of North Pacific deep water during the early Cenozoic, *Geology*, *40*(6), 527–530, doi:10.1130/G32886.1.
Hay, W. W. (2008), Evolving ideas about the Cretaceous climate and ocean circulation, *Cretac. Res.*, *29*(5–6), 725–753, doi:10.1016/j.cretres.2008.05.025.
Hay, W. W. (2011), Can humans force a return to a "Cretaceous" climate?, *Sediment. Geol.*, *235*(1–2), 5–26, doi:10.1016/j.sedgeo.2010.04.015.
Hay, W. W., and S. Floegel (2012), New thoughts about the cretaceous climate and oceans, *Earth Sci. Rev.*, *115*(4), 262–272, doi:10.1016/j.earscirev.2012.09.008.
Hay, W. W., R. M. DeConto, and C. N. Wold (1997), Climate: Is the past the key to the future?, *Int. J. Earth Sci.*, *86*(2), 471–491, doi:10.1007/s005310050155.
Haywood, A. M., et al. (2013), Large-scale features of Pliocene climate: Results from the Pliocene model Intercomparison project, *Clim. Past*, *9*, 191–209, doi:10.5194/cp-9-191-2013.
Heinemann, M., J. H. Jungclaus, and J. Marotzke (2009), Warm Paleocene/Eocene climate as simulated in ECHAM5/MPI-OM, *Clim. Past*, *5*, 785–802, doi:10.5194/cp-5-785-2009.
Herman, A. B., R. A. Spicer, and T. E. Spicer (2016), Environmental constraints on terrestrial vertebrate behaviour and reproduction in the high Arctic of the Late Cretaceous, *Palaeogeogr. Palaeoclimatol. Palaeoecol.*, *441*, 317–338, doi:10.1016/j.palaeo.2015.09.041.
Hibler, W. D. (1979), A dynamic thermodynamic sea ice model, *J. Phys. Oceanogr.*, *9*(4), 815–846, doi:10.1175/1520-0485(1979)009<0815:ADTSIM>2.0.CO;2.
Ho, S. L., and T. Laepple (2016), Flat meridional temperature gradient in the early Eocene in the subsurface rather than surface ocean, *Nat. Geosci.*, *9*(8), 606–610, doi:10.1038/ngeo2763.
Huang, X., M. Stärz, K. Gohl, G. Knorr, and G. Lohmann (2017), Impact of Weddell Sea shelf progradation on Antarctic bottom water formation during the Miocene, *Paleoceanography*, *32*, 304–317, doi:10.1002/2016PA002987.
Huber, M., and E. Thomas (2009), Paleoceanography: The greenhouse world, in *Elements of Physical Oceanography: A Derivative of the Encyclopedia of Ocean Sciences*, pp. 4229–4239, Academic Press, London, U. K.
Huber, M., and R. Caballero (2011), The early Eocene equable climate problem revisited, *Clim. Past*, *7*(2), 603, doi:10.5194/cp-7-603-2011.
Hunter, S. J., P. J. Valdes, A. M. Haywood, and P. J. Markwick (2008), Modelling Maastrichtian climate: Investigating the role of geography, atmospheric CO_2 and vegetation, *Clim. Past Discuss.*, *4*(4), 981–1019, doi:10.5194/cpd-4-981-2008.
Hunter, S. J., A. M. Haywood, P. J. Valdes, J. E. Francis, and M. J. Pound (2013), Modelling equable climates of the Late Cretaceous: Can new boundary conditions resolve data–model discrepancies?, *Palaeogeogr. Palaeoclimatol. Palaeoecol.*, *392*, 41–51, doi:10.1016/j.palaeo.2013.08.009.
Ingalls, A. E. (2016), Palaeoceanography: Signal from the subsurface, *Nat. Geosci.*, *9*(8), 572–573, doi:10.1038/ngeo2765.
Jenkyns, H. C., A. Forster, S. Schouten, and J. S. S. Damsté (2004), High temperatures in the Late Cretaceous Arctic Ocean, *Nature*, *432*(7019), 888–892, doi:10.1038/nature03143.
Kiehl, J. T., and C. A. Shields (2013), Sensitivity of the Palaeocene–Eocene thermal maximum climate to cloud properties, *Philos. Trans. R. Soc. London, Ser. A*, *371*(2001), 20130093, doi:10.1098/rsta.2013.0093.
Knorr, G., and G. Lohmann (2014), Climate warming during Antarctic ice sheet expansion at the middle Miocene transition, *Nat. Geosci.*, *7*, 376–381, doi:10.1038/ngeo2119.
Knorr, G., M. Butzin, A. Micheels, and G. Lohmann (2011), A warm Miocene climate at low atmospheric CO_2 levels, *Geophys. Res. Lett.*, *38*, L20701, doi:10.1029/2011GL048873.

Köhler, P., G. Knorr, and E. Bard (2014), Permafrost thawing as a possible source of abrupt carbon release at the onset of the Bølling/Allerød, *Nat. Commun.*, *5*, 5520, doi:10.1038/ncomms6520.
Kowalewski, M. (1996), Time-averaging, over completeness, and the geological record, *J. Geol.*, *104*(3), 317–326, doi:10.1086/629827.
Kump, L. R., and D. Pollard (2008), Amplification of cretaceous warmth by biological cloud feedbacks, *Science*, *320*(5873), 195–195, doi:10.1126/science.1153883.
Laskar, J., P. Robutel, F. Joutel, M. Gastineau, A. C. M. Correia, and B. Levrard (2004), A long-term numerical solution for the insolation quantities of the earth, *Astron. Astrophys.*, *428*(1), 261–285, doi:10.1051/0004-6361:20041335.
Lécuyer, C., R. Amiot, A. Touzeau, and J. Trotter (2013), Calibration of the phosphate δ18O thermometer with carbonate–water oxygen isotope fractionation equations, *Chem. Geol.*, *347*, 217–226, doi:10.1016/j.chemgeo.2013.03.008.
Lefebvre, V., Y. Donnadieu, Y. Goddéris, F. Fluteau, and L. Hubert-Théou (2013), Was the Antarctic glaciation delayed by a high degassing rate during the early Cenozoic?, *Earth Planet. Sci. Lett.*, *371–372*, 203–211, doi:10.1016/j.epsl.2013.03.049.
Linnert, C., S. A. Robinson, J. A. Lees, P. R. Bown, I. Pérez-Rodríguez, M. R. Petrizzo, F. Falzoni, K. Littler, J. A. Arz, and E. E. Russell (2014), Evidence for global cooling in the Late Cretaceous, *Nat. Commun.*, *5*, 4194, doi:10.1038/ncomms5194.
Little, S. A., S. W. Kembel, and P. Wilf (2010), Paleotemperature proxies from leaf fossils reinterpreted in light of evolutionary history, *PLoS One*, *5*(12), e15161, doi:10.1371/journal.pone.0015161.
Lohmann, G., M. Pfeiffer, T. Laepple, G. Leduc, and J.-H. Kim (2013), A model–data comparison of the Holocene global sea surface temperature evolution, *Clim. Past*, *9*, 1807–1839, doi:10.5194/cp-9-1807-2013.
Lunt, D. J., et al. (2012), A model–data comparison for a multi-model ensemble of early Eocene atmosphere–ocean simulations: EoMIP, *Clim. Past*, *8*, 1717–1736, doi:10.5194/cp-8-1717-2012.
Lunt, D. J., A. Farnsworth, C. Loptson, G. L. Foster, P. Markwick, C. L. O'Brien, R. D. Pancost, S. A. Robinson, and N. Wrobel (2016), Palaeogeographic controls on climate and proxy interpretation, *Clim. Past*, *12*, 1181–1198, doi:10.5194/cp-12-1181-2016.
Markwick, P. J. (2007), The palaeogeographic and palaeoclimatic significance of climate proxies for data-model comparisons, in deep-time perspectives on climate change: Marrying the signal from computer models and biological proxies, in *The Micropalaeontological Society Special Publications*, pp. 251–312, The Geological Society, London.
Markwick, P. J., and P. J. Valdes (2004), Palaeo-digital elevation models for use as boundary conditions in coupled ocean–atmosphere GCM experiments: A Maastrichtian (late Cretaceous) example, *Palaeogeogr. Palaeoclimatol. Palaeoecol.*, *213*(1–2), 37–63, doi:10.1016/j.palaeo.2004.06.015.
Marsland, S. J., H. Haak, J. H. Jungclaus, M. Latif, and F. Röske (2003), The Max-Planck-Institute global ocean/sea ice model with orthogonal curvilinear coordinates, *Ocean Model.*, *5*(2), 91–127, doi:10.1016/S1463-5003(02)00015-X.
Moiroud, M., E. Pucéat, Y. Donnadieu, G. Bayon, K. Moriya, J. F. Deconinck, and M. Boyet (2013), Evolution of the neodymium isotopic signature of neritic seawater on a northwestern Pacific margin: New constrains on possible end-members for the composition of deep-water masses in the Late Cretaceous ocean, *Chem. Geol.*, *356*, 160–170, doi:10.1016/j.chemgeo.2013.08.008.
Monteiro, F. M., R. D. Pancost, A. Ridgwell, and Y. Donnadieu (2012), Nutrients as the dominant control on the spread of anoxia and euxinia across the Cenomanian-Turonian oceanic anoxic event (OAE2): Model-data comparison, *Paleoceanography*, *27*, PA4209, doi:10.1029/2012PA002351.
Otto-Bliesner, B. L., and G. R. Upchurch Jr. (1997), Vegetation-induced warming of high-latitude regions during the Late Cretaceous period, *Nature*, *385*(6619), 804.
Otto-Bliesner, B. L., E. C. Brady, and C. Shields (2002), Late Cretaceous ocean: Coupled simulations with the National Center for Atmospheric Research climate system model, *J. Geophys. Res.*, *107*(D2), 4019, doi:10.1029/2001JD000821.
Ounis, A., L. Kocsis, F. Chaabani, and H.-R. Pfeifer (2008), Rare earth elements and stable isotope geochemistry (δ13C and δ18O) of phosphorite deposits in the Gafsa Basin, Tunisia, *Palaeogeogr. Palaeoclimatol. Palaeoecol.*, *268*(1–2), 1–18, doi:10.1016/j.palaeo.2008.07.005.
Pearson, P. N., P. W. Ditchfield, J. Singano, K. G. Harcourt-Brown, C. J. Nicholas, R. K. Olsson, N. J. Shackleton, and M. A. Hall (2001), Warm tropical sea surface temperatures in the Late Cretaceous and Eocene epochs, *Nature*, *413*(6855), 481–487, doi:10.1038/35097000.
Peppe, D. J., et al. (2011), Sensitivity of leaf size and shape to climate: Global patterns and paleoclimatic applications, *New Phytol.*, *190*(3), 724–739, doi:10.1111/j.1469-8137.2010.03615.x.
Pfeiffer, M., and G. Lohmann (2016), Greenland ice sheet influence on last interglacial climate: Global sensitivity studies performed with an atmosphere–ocean general circulation model, *Clim. Past*, *12*, 1313–1338, doi:10.5194/cp-12-1313-2016.
Poulsen, C. J., and J. Zhou (2013), Sensitivity of Arctic climate variability to mean state: Insights from the cretaceous, *J. Clim.*, *26*(18), 7003–7022, doi:10.1175/JCLI-D-12-00825.1.
Poulsen, C. J., A. S. Gendaszek, and R. L. Jacob (2003), Did the rifting of the Atlantic Ocean cause the cretaceous thermal maximum?, *Geology*, *31*(2), 115–118, doi:10.1130/0091-7613(2003)031<0115:DTROTA>2.0.CO;2.
Pucéat, E., Y. Donnadieu, G. Ramstein, F. Fluteau, and F. Guillocheau (2005), Numerical evidence for thermohaline circulation reversals during the Maastrichtian, *Geochem. Geophys. Geosyst.*, *6*, Q11012, doi:10.1029/2005GC000998.
Pucéat, E., C. Lécuyer, Y. Donnadieu, P. Naveau, H. Cappetta, G. Ramstein, B. T. Huber, and J. Kriwet (2007), Fish tooth δ18O revising Late Cretaceous meridional upper ocean water temperature gradients, *Geology*, *35*(2), 107–110, doi:10.1130/G23103A.1.
Pucéat, E., et al. (2010), Revised phosphate–water fractionation equation reassessing paleotemperatures derived from biogenic apatite, *Earth Planet. Sci. Lett.*, *298*(1–2), 135–142, doi:10.1016/j.epsl.2010.07.034.
Retallack, G. J. (1998), Fossil soils and completeness of the rock and fossil record, in *The Adequacy of the Fossil Record*, pp. 133–163, Wiley-Blackwell, New Jersey.
Roberts, C. D., A. N. LeGrande, and A. K. Tripati (2009), Climate sensitivity to Arctic seaway restriction during the early Paleogene, *Earth Planet. Sci. Lett.*, *286*(3–4), 576–585, doi:10.1016/j.epsl.2009.07.026.
Roeckner, E., et al. (2003), The atmospheric general circulation model ECHAM 5. PART I: Model description, *Report 349*, Max-Planck Institut für Meteorologie, Hamburg.
Royer, D. L., M. Pagani, and D. J. Beerling (2012), Geobiological constraints on earth system sensitivity to CO_2 during the cretaceous and Cenozoic, *Geobiology*, *10*(4), 298–310, doi:10.1111/j.1472-4669.2012.00320.x.
Schneider, B., G. Leduc, and W. Park (2010), Disentangling seasonal signals in Holocene climate trends by satellite-model-proxy integration, *Paleoceanography*, *25*, PA4217, doi:10.1029/2009PA001893.
Schouten, S., E. C. Hopmans, A. Forster, Y. van Breugel, M. M. M. Kuypers, and J. S. S. Damsté (2003), Extremely high sea-surface temperatures at low latitudes during the middle Cretaceous as revealed by archaeal membrane lipids, *Geology*, *31*(12), 1069–1072, doi:10.1130/G19876.1.
Schröder-Adams, C. (2014), The Cretaceous Polar and Western Interior seas: Paleoenvironmental history and paleoceanographic linkages, *Sediment. Geol.*, *301*, 26–40, doi:10.1016/j.sedgeo.2013.12.003.

Sellwood, B. W., and P. J. Valdes (2006), Mesozoic climates: General circulation models and the rock record, *Sediment. Geol.*, *190*(1–4), 269–287, doi:10.1016/j.sedgeo.2006.05.013.
Setoyama, E., M. A. Kaminski, and J. Tyszka (2011a), The Late Cretaceous–Early Paleocene palaeobathymetric trends in the southwestern Barents Sea—Palaeoenvironmental implications of benthic foraminiferal assemblage analysis, *Palaeogeogr. Palaeoclimatol. Palaeoecol.*, *307*(1–4), 44–58, doi:10.1016/j.palaeo.2011.04.021.
Setoyama, E., M. A. Kaminski, and J. Tyszka (2011b), Campanian agglutinated foraminifera from the Lomonosov ridge, IODP expedition 302, ACEX, in the paleogeographic context of the Arctic Ocean, *Micropaleontology*, *57*, 507–530.
Setoyama, E., W. Radmacher, M. A. Kaminski, and J. Tyszka (2013), Foraminiferal and palynological biostratigraphy and biofacies from a Santonian–Campanian submarine fan system in the Vøring Basin (offshore Norway), *Mar. Pet. Geol.*, *43*, 396–408, doi:10.1016/j.marpetgeo.2012.12.007.
Sewall, J. O., R. S. W. Van de Wal, K. V. D. Zwan, C. V. Oosterhout, H. A. Dijkstra, and C. R. Scotese (2007), Climate model boundary conditions for four cretaceous time slices, *Clim. Past*, *3*(4), 647–657, doi:10.5194/cp-3-647-2007.
Shellito, C. J., L. C. Sloan, and M. Huber (2003), Climate model sensitivity to atmospheric CO_2 levels in the Early–Middle Paleogene, *Palaeogeogr. Palaeoclimatol. Palaeoecol.*, *193*(1), 113–123, doi:10.1016/S0031-0182(02)00718-6.
Shellito, C. J., J. F. Lamarque, and L. C. Sloan (2009), Early Eocene Arctic climate sensitivity to pCO_2 and basin geography, *Geophys. Res. Lett.*, *36*, L09707, doi:10.1029/2009GL037248.
Skelton, P. W. (Ed.) (2003), *The Cretaceous World*, Cambridge Univ. Press, Cambridge, U. K.
Solomon, S., et al. (2007), Technical summary, in *Climate Change 2007: The Physical Science Basis. Contribution of Working Group I to the Fourth Assessment Report of the Intergovernmental Panel on Climate Change*, edited by S. Solomon et al., pp. 19–91, Cambridge Univ. Press, Cambridge, U. K., and New York.
Spicer, R. A., and A. B. Herman (2010), The Late Cretaceous environment of the Arctic: A quantitative reassessment based on plant fossils, *Palaeogeogr. Palaeoclimatol. Palaeoecol.*, *295*(3–4), 423–442, doi:10.1016/j.palaeo.2010.02.025.
Stärz, M., G. Lohmann, and G. Knorr (2016), The effect of a dynamic soil scheme on the climate of the mid-Holocene and the Last Glacial Maximum, *Clim. Past*, *12*(1), 151, doi:10.5194/cp-12-151-2016.
Stärz, M., W. Jokat, G. Knorr, and G. Lohmann (2017), Threshold in North Atlantic-Arctic Ocean circulation controlled by the subsidence of the Greenland-Scotland ridge, *Nat. Commun.*, *8*, 15681, doi:10.1038/ncomms15681.
Stein, R., et al. (2016), Evidence for ice-free summers in the late Miocene central Arctic Ocean, *Nat. Commun.*, *7*, 11148, doi:10.1038/ncomms11148.
Stepanek, C., and G. Lohmann (2012), Modelling mid-Pliocene climate with COSMOS, *Geosci. Model Dev.*, *5*, 1221–1243, doi:10.5194/gmd-5-1221-2012.
Tarduno, J. A., D. B. Brinkman, P. R. Renne, R. D. Cottrell, H. Scher, and P. Castillo (1998), Evidence for extreme climatic warmth from Late Cretaceous Arctic vertebrates, *Science*, *282*(5397), 2241–2243, doi:10.1126/science.282.5397.2241.
Upchurch, G. R., B. L. Otto-Bliesner, and C. R. Scotese (1999), Terrestrial vegetation and its effects on climate during the latest Cretaceous, *Geol. Soc. Am. Spec. Pap.*, *332*, 407–426, doi:10.1130/0-8137-2332-9.407.
Upchurch, G. R., J. Kiehl, C. Shields, J. Scherer, and C. Scotese (2015), Latitudinal temperature gradients and high-latitude temperatures during the latest Cretaceous: Congruence of geologic data and climate models, *Geology*, *43*(8), 683–686, doi:10.1130/G36802.1.
Valcke, S. (2013), The OASIS3 coupler: A European climate modelling community software, *Geosci. Model Dev.*, *6*(2), 373–388, doi:10.5194/gmd-6-373-2013.
Walliser, E. O., G. Lohmann, I. Niezgodzki, T. Tütken, and B. R. Schöne (2016), Response of central European SST to atmospheric pCO_2 forcing during the Oligocene—A combined proxy data and numerical climate model approach, *Palaeogeogr. Palaeoclimatol. Palaeoecol.*, *459*, 552–569, doi:10.1016/j.palaeo.2016.07.033.
Wei, W., and G. Lohmann (2012), Simulated Atlantic multidecadal oscillation during the Holocene, *J. Clim.*, *25*(20), 6989–7002, doi:10.1175/JCLI-D-11-00667.1.
Wei, W., G. Lohmann, and M. Dima (2012), Distinct modes of internal variability in the global meridional overturning circulation associated with the Southern Hemisphere westerly winds, *J. Phys. Oceanogr.*, *42*(5), 785–801, doi:10.1175/JPO-D-11-038.1.
Werner, M., P. M. Langebroek, T. Carlsen, M. Herold, and G. Lohmann (2011), Stable water isotopes in the ECHAM5 general circulation model: Toward high-resolution isotope modeling on a global scale, *J. Geophys. Res.*, *116*, D15109, doi:10.1029/2011JD015681.
Winguth, A., C. Shellito, C. Shields, and C. Winguth (2010), Climate response at the Paleocene-Eocene thermal maximum to greenhouse gas forcing—A model study with CCSM3, *J. Clim.*, *23*(10), 2562–2584, doi:10.1175/2009JCLI3113.1.
Wolfe, J. A., and G. R. Upchurch (1987), North American nonmarine climates and vegetation during the Late Cretaceous, *Palaeogeogr. Palaeoclimatol. Palaeoecol.*, *61*, 33–77, doi:10.1016/0031-0182(87)90040-X.
Zhang, X., G. Lohmann, G. Knorr, and X. Xu (2013), Different ocean states and transient characteristics in Last Glacial Maximum simulations and implications for deglaciation, *Clim. Past*, *9*, 2319–2333, doi:10.5194/cp-9-2319-2013.
Zhang, X., G. Lohmann, G. Knorr, and C. Purcell (2014), Abrupt glacial climate shifts controlled by ice sheet changes, *Nature*, *512*(7514), 290–294, doi:10.1038/nature13592.